Mid-Infrared Silicon Photonic Crystal Fiber Polarization Filter Based on Surface Plasmon Resonance Effect

Yuwei Qu[a)] Jinhui Yuan[a)b)*] Xian Zhou[b)] Feng Li[c)] Binbin Yan[a)] Qiang Wu[d)e)*] Kuiru Wang[a)] Xinzhu Sang[a)] Keping Long[b)] Chongxiu Yu[a)]

a State Key Laboratory of Information Photonics and Optical Communications, Beijing University of Posts and Telecommunications, Beijing 100876, China

b Research Center for Convergence Networks and Ubiquitous Services, University of Science & Technology Beijing (USTB), Beijing 100083, China

c Photonics Research Centre, Department of Electronic and Information Engineering, The Hong Kong Polytechnic University, Hung Hom, Hong Kong

d Department of Physics and Electrical Engineering, Northumbria University, Newcastle upon Tyne, NE1 8ST, United Kingdom

e Key Laboratory of Nondestructive Test (Ministry of Education), Nanchang Hangkong University, Nanchang 330063, China

**yuanjinhui81@bupt.edu.cn; qiang.wu@northumbria.ac.uk*

ABSTRACT In this paper, a novel silicon photonic crystal fiber (Si-PCF) polarization filter based on surface plasmon resonance effect is proposed for the first time. With the full-vector finite-element method, the mode coupling characteristics of the Si-PCF with the gold-coated film between the core mode and surface plasmon polariton mode are investigated, and the confinement losses are analyzed. The confinement losses of the Y-polarized core mode at the three resonant wavelengths 2.84, 3.29, and 4.53 μm are 9235.9, 27097.5, and 97818.3 dB/m, respectively. The extinction ratio reaches -391 dB and the insertion loss is less than 1 dB when the Si-PCF length is 4 mm, along with the filter bandwidth of 2.75 μm. Moreover, by modifying the fiber structure parameters, the filter bandwidth of the proposed three kinds of Si-PCF polarization filters can cover 2.75 to 7.80 μm. It is believed that the proposed Si-PCF polarization filter has important applications in the mid-infrared laser and optical communication systems.

Keywords Surface plasmon resonance; silicon photonic crystal fiber; polarization filter; mid-infrared

1. Introduction

In recent years, the photonic crystal fiber (PCF) polarization-related devices and sensors combined with surface plasmon resonance (SPR) effect have become one of the research hotspots [1-6]. Among all of them, the PCF polarization filters designed by the mode coupling mechanism of the PCF core mode and the surface plasmon polariton (SPP) mode are very promising for the laser and optical communication systems [7-13]. In 2017, Yang et al. proposed a single-polarization PCF filter coated with the silver film, where the filtering wavelength can be tunable within a wide wavelength range by filling the liquid into different air holes [14]. In 2018, Li et al. reported a V-type birefringent PCF embedded with the dual copper wires, where the filter bandwidth covered the S+L wave-band [15]. In 2018, Guo et al. demonstrated a D-shaped single-polarization PCF filter and the Y-polarized core mode confinement loss reached 37631 dB/m at the wavelength of 1.55 μm and the filter bandwidth was reached 480 nm [16]. In 2019, Chang et al. discussed a compact PCF polarization filter with two gold-coated air holes, and the Y-polarized core mode confinement loss could be up to 44200 dB/m at the wavelength of 1.55 μm

and the filter bandwidth was reached 300 nm [17]. However, all the PCF polarization filters reported are based on the PCF fabricated with the silica material, whose transmission window is limited to the near-infrared spectral region.

Compared with the silica PCF, the PCF fabricated with the silicon material has good transmission characteristics in the mid-infrared spectral region [18, 19]. In 2009, Yaman et al. had successfully fabricated the silicon PCF (Si-PCF) using the magnesiothermic reduction method [20, 21]. In 2014, Huang et al. reported a large birefringence and high nonlinearity spiral Si-PCF [22]. In 2017, Liao et al. designed a Si-PCF with ultra-flattened nearly-zero dispersion [23]. The Si-PCFs with the different optical characteristics have potential applications in realizing mid-infrared photonic devices, such as modulator, filter, and so on. However, the research on SPR-Si-PCF polarization filter has not been reported.

In this paper, we propose a novel Si-PCF polarization filter based on the mode coupling mechanism of the PCF core mode and the SPP mode for the first time. The mode coupling and confinement loss characteristics of the Si-PCF are analyzed with the full-vector finite-element method. Three kinds of mid-infrared Si-PCF polarization filters have different bandwidth are obtained. Furthermore, the extinction ratio, insertion loss, and error-tolerant rate are discussed.

2. Design of the Si-PCF Polarization Filter

The cross-section structure of the designed Si-PCF polarization filter is shown in Fig. 1. From Fig. 1, the matrix material of the Si-PCF is the silicon, and hole to hole space is Λ. The Si-PCF contains the three layers of air holes, which are arranged in regular hexagonal lattice. The two larger air holes with diameter of d_2 are introduced in the X-direction, which destroys the symmetry of the cladding structure and causes the mode birefringence, making the Y-polarized core mode more easily coupled with the SPP mode. In order to enhance the coupling effect between the Y-polarized core mode and SPP mode, a larger air hole with diameter of d_3 in the Y-direction is coated with the gold film, whose thickness is t. The gold material has stable chemical property, good biomolecular compatibility, and strong corrosion resistance. When the light is propagated inside the Si-PCF coated with the gold film, the free electrons on the gold film surface interact with the incident light field, forming the surface plasma resonance. And the diameters of the other air holes are d_1. Perfect matching layer (PML) is used at the outermost edge of the designed Si-PCF so as to absorb the radiation energy [24].

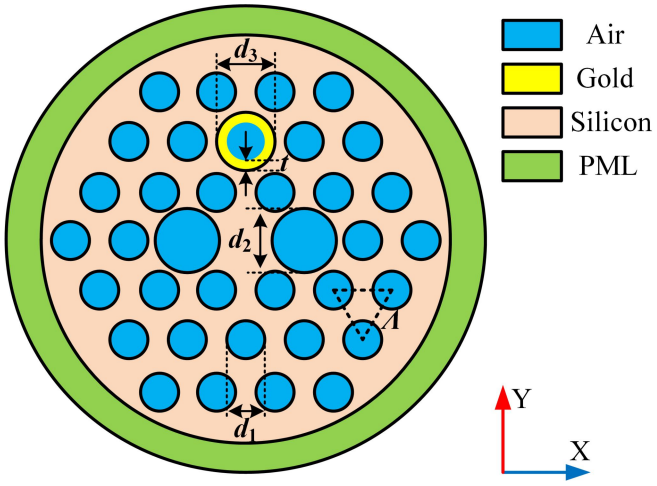

Fig. 1. The cross-section of the designed Si-PCF polarization filter.

The full-vector finite-element method (FV-FEM) is used to investigate the mode coupling characteristic between the designed Si-PCF core mode and the SPP mode. The material dispersion of the silicon can be calculated by the Sellmeier equation [25]

$$n_{\mathrm{Si}}(\lambda)=\varepsilon+\frac{\mathrm{A}}{\lambda^2}+\frac{\mathrm{B}\,\lambda_1^2}{\lambda^2-\lambda_1^2}, \tag{1}$$

where λ_1=1.1071 μm, ε=11.6858, A=0.939816 μm^2, and B=8.10461×10^{-3}.

The relative dielectric constant of the gold can be calculated by Drude-Lorentz model [26]

$$\varepsilon_{\mathrm{m}}=\varepsilon_{\infty}-\frac{\omega_{\mathrm{D}}^2}{\omega(\omega-j\gamma_{\mathrm{D}})}-\frac{\Delta\varepsilon\cdot\Omega_{\mathrm{L}}^2}{(\omega^2-\Omega_{\mathrm{L}}^2)-j\Gamma_{\mathrm{L}}\omega}, \tag{2}$$

where ε_∞=5.9673 and $\Delta\varepsilon$=1.09 represent the high frequency dielectric constant and the weighted coefficient, respectively, ω is the angle frequency of the guided-wave, ω_{D} is the plasma frequency, γ_{D} is the damping frequency, Ω_{L} is the frequency of the Lorentz oscillator and Γ_{L} is the bandwidth of the Lorentz oscillator. Here, $\omega_{\mathrm{D}}/2\pi$=2113.6 THz, $\gamma_{\mathrm{D}}/2\pi$=15.92 THz, $\Omega_{\mathrm{L}}/2\pi$=650.07 THz, and $\Gamma_{\mathrm{L}}/2\pi$=104.86 THz.

The confinement loss (L_{C}) can be expressed by [27]

$$L_{\mathrm{C}}=\frac{20}{\ln 10}\frac{2\pi}{\lambda}\mathrm{Im}[n_{\mathrm{eff}}]\times 10^6, \tag{3}$$

where the Im(n_{eff}) is the imaginary part of the effective refractive index of the core mode.

The confinement loss ratio (CLR) can be calculated by

$$\mathrm{CLR}=\frac{L_{\mathrm{CY}}}{L_{\mathrm{CX}}}, \tag{4}$$

where L_{CX} and L_{CY} are the confinement losses of the X-polarized and Y-polarized core modes, respectively.

The normalized output powers P_{out} of the X-polarized and Y-polarized core modes are calculated as [28]

$$P_{\mathrm{out}}(x,y)=P_{\mathrm{in}}(x,y)\exp(-L_{\mathrm{c}}(x,y)(\frac{\ln 10}{10})L), \tag{5}$$

where $P_{\mathrm{in}}(x, y)$ and L are the input power and fiber length, respectively.

The extinction ratio (ER) and insertion loss (IL) as the two important parameters for evaluating the filter performance can be described by [28, 29]

$$ER=10\log_{10}\frac{P_{out}(x)}{P_{out}(y)}, \tag{6}$$

$$IL_x=-10\log_{10}\frac{P_{out}(x)}{P_{in}}, \tag{7}$$

3. Numerical Results and Analysis

The real part Re(n_{eff}) of the effective refractive index of the X-polarized and the Y-polarized core modes and the SPP modes as seen from Fig. 2 when the structure parameters of the Si-PCF are chosen as following: d_1=1.30 μm, d_2=2.64 μm, d_3=2.16 μm, Λ=2.1 μm, and t=50 nm. Based on the coupled-mode theory [30, 31], the complete coupling between the Y-polarized core mode and the first-order SPP mode occurs at the resonant wavelength 4.53 μm, while at the resonant wavelengths 2.84 and 3.29 μm, the incomplete coupling between the Y-polarized core mode and the third-order and the second-order SPP modes occur, respectively, as seen from Fig. 2(a). In contrast, there is no coupling between the X-polarized core mode and different-order SPP modes. In order to clearly show the coupling between the Y-polarized core mode and the different-order

SPP modes, the electric field distributions of the Y-polarized core mode at the three resonant wavelengths are shown in Figs. 2(b), 2(c), and 2(d), respectively. From Figs. 2(b) and 2(c), the weak energy transductions between the Y-polarized core mode and the third-order and the second-order SPP modes occur at the resonant wavelengths 2.84 and 3.29 μm, respectively. While at the resonant wavelength 4.53 μm, the strong energy transfer between the Y-polarized core mode and the first-order SPP mode occurs, as seen from Fig. 2(d).

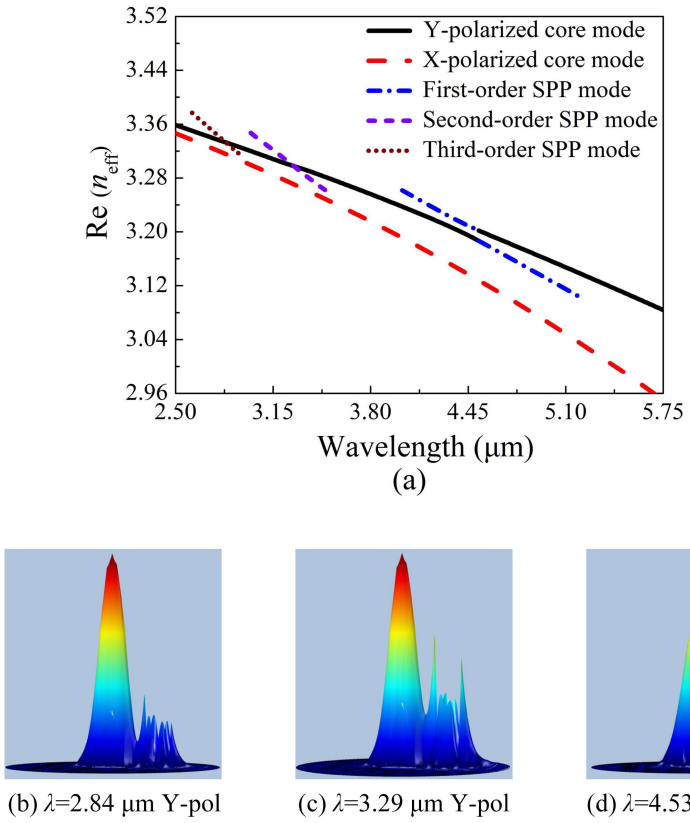

Fig. 2. The real part Re(n_{eff}) **(a)** of the effective refractive indices of the X-polarized and the Y-polarized core modes and the SPP modes. **(b)**, **(c)**, and **(d)** show the electric field distributions of the Y-polarized core mode at the three resonant wavelengths 2.84, 3.29, and 4.53 μm, respectively.

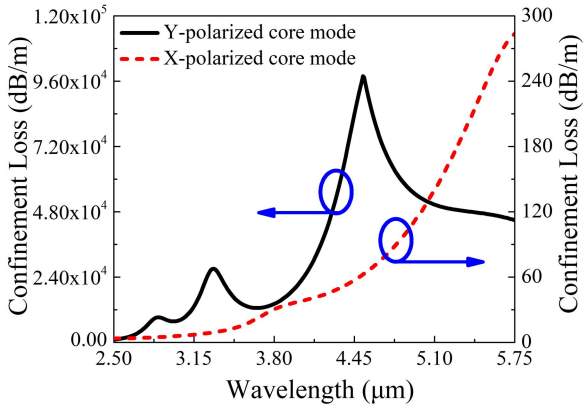

Fig. 3. The confinement losses of the Y-polarized and X-polarized core modes of the designed Si-PCF.

Because of the coupling between the Y-polarized core mode and the SPP modes, the confinement loss of the Y-polarized core mode increases sharply, and it will be completely lost

after a short propagation. At this time, the filtering effect can be obtained because only the X-polarized core mode is retained. The filtering performance is good when the mode coupling between the Y-polarized core mode and the SPP modes is strong. The confinement losses of the X-polarized and the Y-polarized core modes of the designed Si-PCF are given out in Fig. 3. It can be seen that the confinement losses of the two modes at the three resonant wavelengths 2.84, 3.29, and 4.53 μm are 9235.9, 27097.5, and 97818.3 dB/m, and 4.83, 9.2, and 62.4 dB/m, respectively.

For the designed Si-PCF polarization filter, it is expected that the confinement loss of the Y-polarized core mode is large enough while the confinement loss of the X-polarized core mode is small enough. Therefore, the CLR between the Y-polarized core mode and the X-polarized core mode of the designed Si-PCF is shown in Fig. 4. The wavelength ranges corresponding to the CLR of the Y-polarized and the X-polarized core modes from Fig. 4 are given out in the Table 1. From Fig. 4 and Table 1, when the CLR of the Y-polarized and X-polarized core modes are larger than 100, 200, and 300 times, the corresponding wavelength ranges are from 2.5 to 5.75 μm, 2.5 to 5.5 μm, and 2.52 to 5.21 μm, respectively. In addition, from Table 1, the wavelength range of the designed Si-PCF polarization filter becomes narrower as the CLR increases. However, if the CLR is very small, the filtering characteristic will also be affected. To achieve the broadband filtering, the CLR > 200 times should be satisfied. At this time, the maximum confinement loss of the X-polarized core mode is only 234.2 dB/m at 5.5 μm.

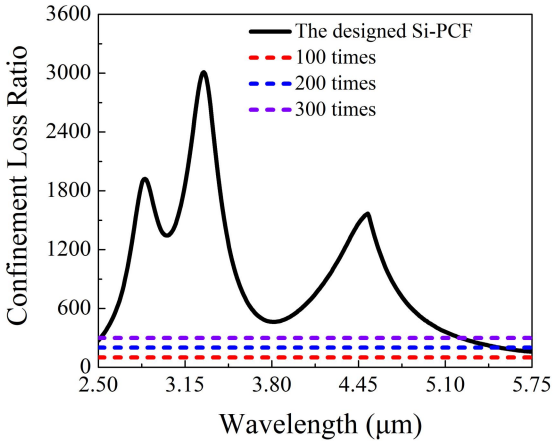

Fig. 4. The CLR of the Y-polarized and the X-polarized core modes of the designed Si-PCF.

Table 1. Wavelength Ranges Corresponding to the CLR of the Y-polarized and the X-polarized Core Modes.

CLR	Wavelength ranges of the designed Si-PCF (μm)
CLR > 100 times	2.50~5.75
CLR > 200 times	2.50~5.50
CLR > 300 times	2.52~5.21

Moreover, the *ER* and the *IL* are shown in Figs. 5(a) and 5(b) when the Si-PCF length *L* increases from 2, to 4, to 6, and to 8 mm, respectively. From Figs. 5(a) and 5(b), as *L* increases, the *ER* and the *IL* become larger. Therefore, it is necessary to choose a suitable Si-PCF length *L* to simultaneously obtain a larger *ER* and smaller *IL*. Thus, the final selection of *L* is 4 mm. For *L*=4 mm, the maximum peak value of the *ER* reaches -391 dB and the effective wavelength range of

the *ER* below -20 dB is from 2.75 to 5.75 μm. Therefore, by considering the wavelength range of the CLR > 200 times and the *ER* of < -20 dB comprehensively, the filtering bandwidth is 2.75 μm (from 2.75 to 5.5 μm), and the *IL* is less than 1 dB.

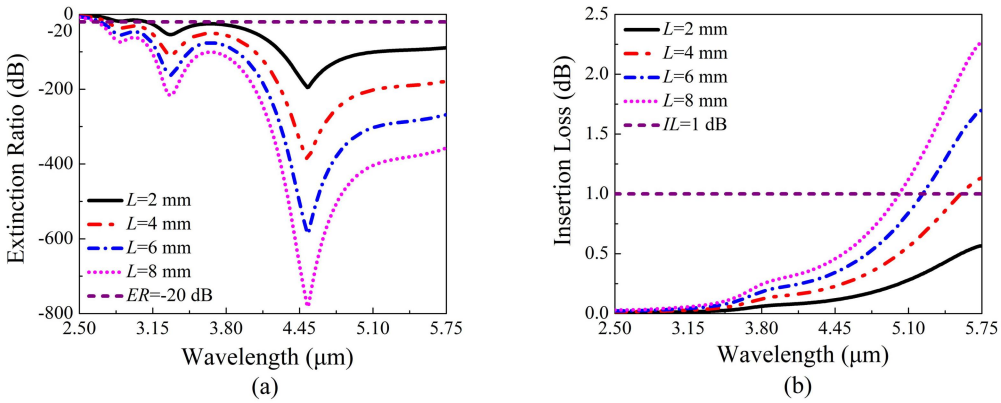

Fig. 5. The *ER* **(a)** and *IL* **(b)** as functions of wavelength for the different Si-PCF lengths.

To further prove the good filtering characteristics of the proposed Si-PCF polarization filter, the relationships between the normalized output power of the X-polarized and Y-polarized core modes at the three resonant wavelengths 2.84, 3.29, and 4.53 μm and *L* are shown in Fig. 6. From Fig. 6, as *L* increases, the normalized output powers of the Y-polarized core mode at 2.84, 3.29, and 4.53 μm drop sharply. When *L* exceeds 3.25 mm, the normalized output powers nearly become zero. The normalized output power of the Y-polarized core mode decreases fastest at 4.53 μm, because the complete coupling between the Y-polarized core mode and first-order SPP mode occurs. However, the normalized output powers of the X-polarized core mode at 2.84, 3.29, and 4.53 μm do not change significantly and remains above 0.94 as *L* increases. Therefore, when the incident light is propagated in a 4 mm long Si-PCF, the Y-polarized core mode is completely lost, and only the X-polarized core mode is left.

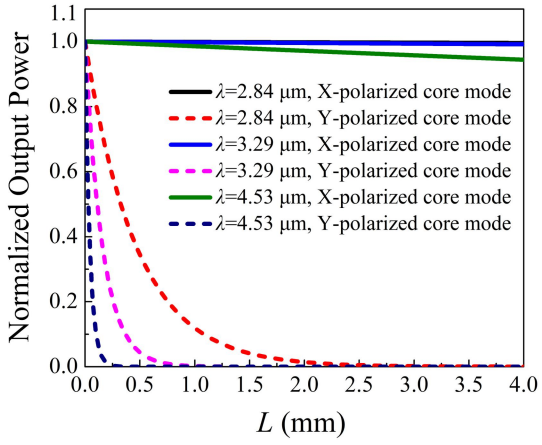

Fig. 6. The relationship between the normalized output power of the X-polarized and Y-polarized core modes at the three resonant wavelengths 2.84, 3.29, and 4.53 μm and *L*.

Table 2 shows the comparison results between the proposed Si-PCF polarization filter and the reported SiO_2-PCF polarization filter. From Table 2, the Si-PCF polarization filter has a maximum *ER*, and the bandwidth of the *ER* below -20 dB is up to 2750 nm. In addition, the *IL* of < 1 dB can meet the actual requirement.

Table 2. Comparison with the reported SiO_2-PCF polarization filters.

Reference	Resonance wavelength	The value of the maximun *ER*	Bandwidth of *ER* below -20 dB	The value of the maximun *IL*
[6] (2019)	1310 nm	Not mentioned	1000 nm	Not mentioned
[17] (2019)	1550 nm	-326 dB	300 nm	Not mentioned
[26] (2019)	1550 nm	-272 dB	138 nm	Not mentioned
[16] (2018)	1550 nm	Not mentioned	Not mentioned	0.22 dB
[28] (2017)	1300 nm	-86.6 dB	850 nm	Not mentioned
[30] (2015)	1270 nm, 1370 nm, 1740 nm	about -68 dB	750 nm	Not mentioned
This work	2840 nm, 3290 nm, 4530nm	-391 dB	2750 nm	Less than 1 dB

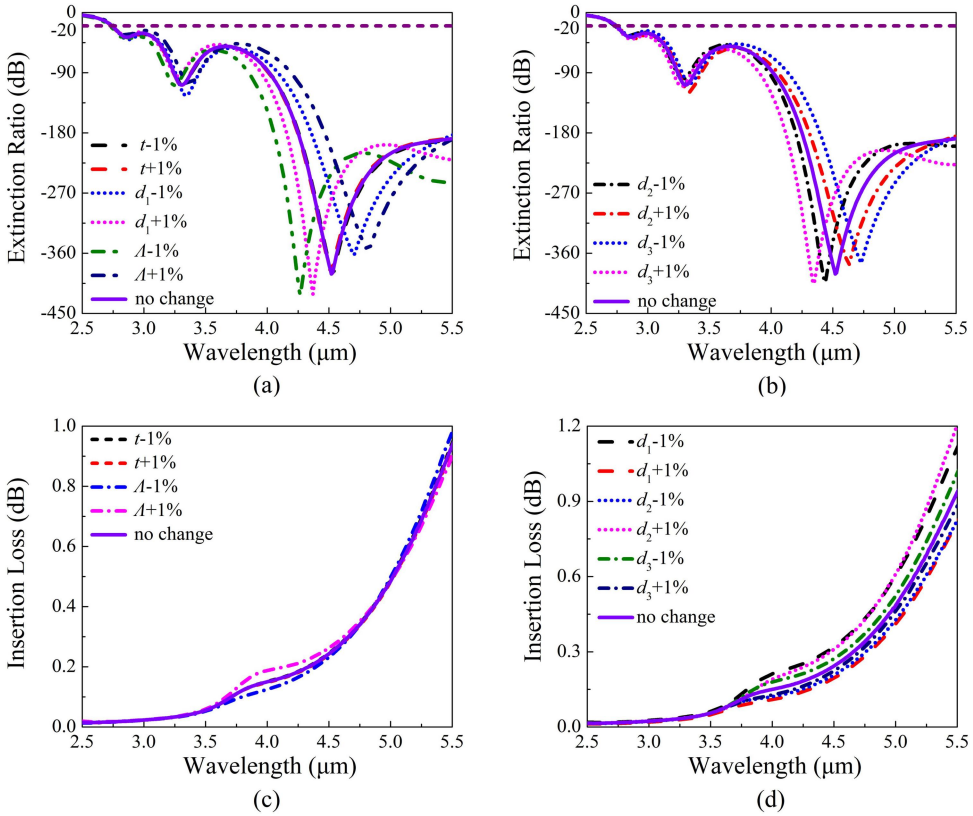

Fig. 7. The *ER* **(a)**, **(b)** and *IL* **(c)**, **(d)** as functions of wavelength when the designed fiber structure parameters Λ, d_1, d_2, d_3, and t have the distortion of ±1%.

For the proposed Si-PCF polarization filter, the required PCF can be fabricated by the ultrasonic or femtosecond laser drilling method [20, 32, 33]. Sputtering or high-pressure microfluidic chemical deposition is usually used for the metal coating [34, 35]. Sputtering coating bombards the surface of the gold material with functional particles, so that the surface atoms of the gold material obtain the enough energy to escape. The sputtered gold material is deposited on the surface of the silicon substrate, forming the gold film. High pressure microfluidic chemical deposition is used to generate the volatile gold gas under high pressure, and then transfer the gold gas to the air hole of PCF so as to form the gold film on silicon substrate. With the two methods,

some works on the gold coating in the PCF air holes are reported [36-39]. At present, the main challenge is the small air hole size. In this work, we coat the gold film on a large air hole. In the actual fabrication, the slight deformation of the Si-PCF structure could occur. The *ER* and *IL* are shown in Figs. 7(a), 7(b), 7(c), and 7(d) when the structure parameters of the Si-PCF d_1, d_2, d_3, Λ, and t change ±1%. From Figs. 7(a) and 7(b), the bandwidth of the *ER* below -20 dB remains nearly unchanged. From Figs. 7(c) and 7(d), the maximum *IL* is only 1.2 dB within the considered wavelength range. These results shown in Figs. 7(a) to 7(d) indicate that the proposed Si-PCF polarization filter has good error-tolerant rate.

4. Design of other Si-PCF Polarization Filters with Different Bandwidths

Figs. 8(a), 8(b), 8(c), and 8(d) show the relationships between the confinement losses of the Y-polarized core mode and changes of the fiber structure parameters d_1, d_2, d_3, and Λ. Because the fiber structure parameters have different influences on Re(n_{eff}) of the Y-polarized core mode and SPP modes, the changes of them can determine the resonant position, coupling strength, and resonant peak number. It can be seen from Figs. 8(a), 8(c), and 8(d) that with the increase of d_1 or d_3, or decrease of Λ, each confinement loss peak of the Y-polarized core mode shifts toward the shorter wavelength, and the number of the confinement loss peaks increases gradually. When the third-order or second-order SPP mode is coupled with the Y-polarized core mode at different resonant wavelengths, the confinement loss peak value of the Y-polarized core mode changes slightly. In contrast, while when the first-order or zero-order SPP mode is coupled with the Y-polarized core mode at different resonant wavelengths, the confinement loss peak value of the

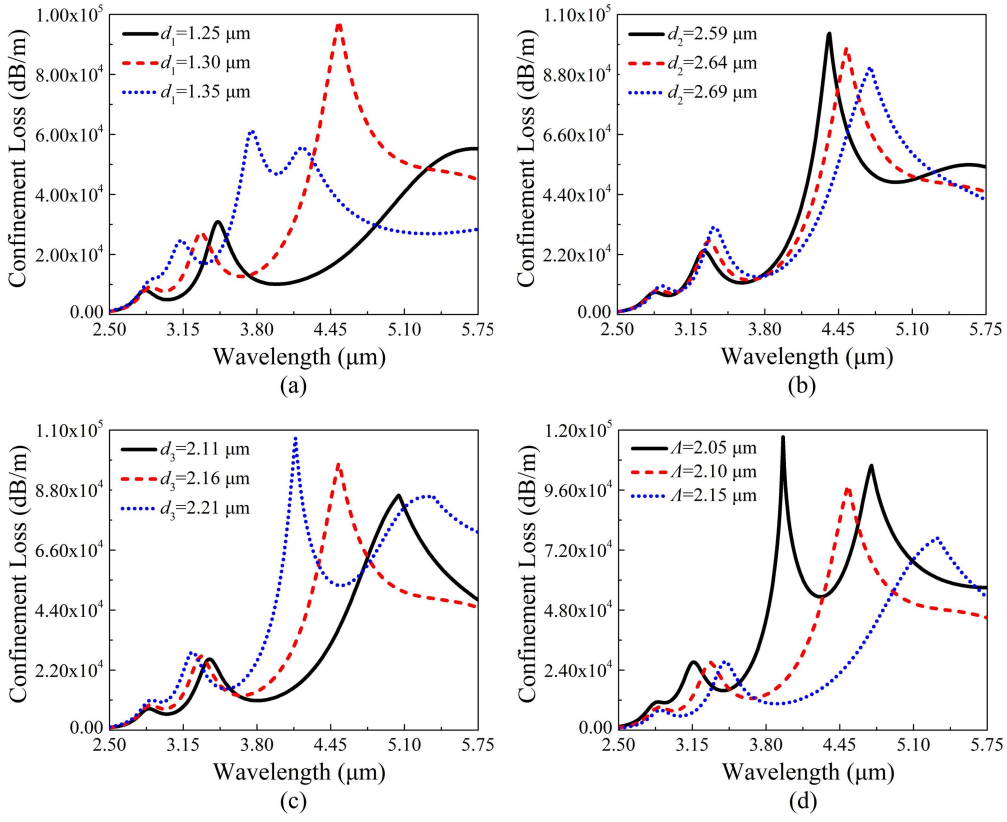

Fig. 8. The relationship between the confinement losses of the Y-polarized core mode and changes of **(a)** d_1, **(b)** d_2, **(c)** d_3, and **(d)** Λ.

Y-polarized core mode changes greatly. From Fig. 8 (b), as d_2 increases, each confinement loss peak of the Y-polarized core mode shifts toward the longer wavelength. Although the wavelength shift range is small, the number of the confinement loss peaks remains unchanged, and the confinement loss peak value does not occur to change evidently. Therefore, it is concluded that the change of d_2 has little effect on the resonant coupling between the Y-polarized core mode and SPP modes. It is better to adjust d_1, d_3, and Λ to achieve different filtering bandwidths.

Based on the above analysis, we choose the two groups of structure parameters as following: Λ=2.5 μm, d_1=1.55 μm, d_2=3.12 μm, d_3=2.58 μm, and t=50 nm, and Λ=3.0 μm, d_1=1.82 μm, d_2=3.72 μm, d_3=3.09 μm, and t=50 nm. At this time, the corresponding Si-PCF is called as Si-PCF-1 and Si-PCF-2, respectively.

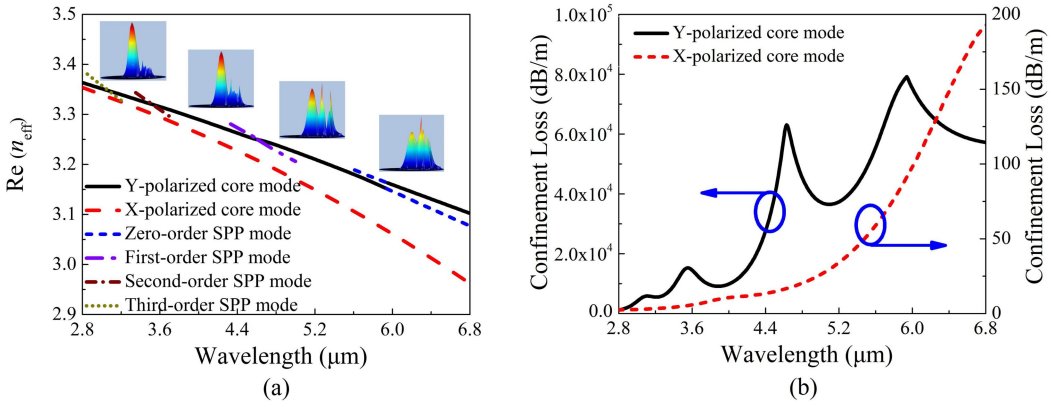

Fig. 9. (a) Re(n_{eff}) of the Y-polarized core mode and SPP modes, and **(b)** the confinement losses of the Y-polarized and X-polarized core modes of the Si-PCF-1. The insets of **(a)** show the electric field distributions of the Y-polarized core mode at different resonant wavelengths.

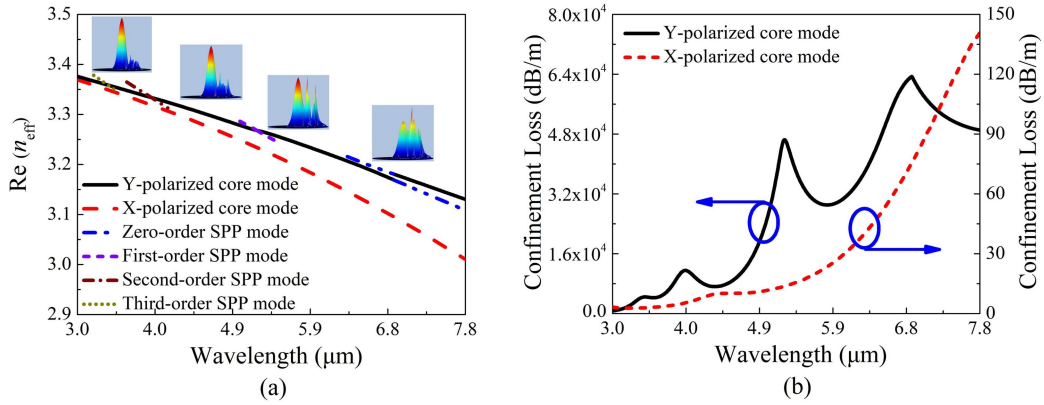

Fig. 10. (a) Re(n_{eff}) of the Y-polarized and X-polarized core modes and SPP modes, and **(b)** the confinement losses of the Y-polarized and X-polarized core modes of the Si-PCF-2. The insets of **(a)** show the electric field distributions of the Y-polarized core mode at different resonant wavelengths.

Re(n_{eff}) of the Y-polarized and the X-polarized core mode and the SPP modes and the confinement loss of the Y-polarized and the X-polarized core modes of the Si-PCF-1 and the Si-PCF-2 are shown in Figs. 9(a) and 9(b) and Figs. 10(a) and 10(b), respectively. From Figs. 9(a) and 10(a), the complete coupling between the Y-polarized core mode and the zero-order and the first-order SPP modes of the Si-PCF-1 and the Si-PCF-2 occurs at the resonant wavelengths 5.95, 4.62, 6.92, and 5.22 μm, respectively. Meanwhile, the incomplete coupling between the Y-polarized core mode and the second-order and the third-order SPP modes of the Si-PCF-1 and

the Si-PCF-2 occurs at the resonant wavelengths 3.53, 3.08, 3.92, and 3.40 μm, respectively. There is also no coupling between the X-polarized core mode and different-order SPP modes. From Figs. 9(b) and 10(b), the Y-polarized core modes of the Si-PCF-1 and the Si-PCF-2 generate the four strong resonant peaks in the considered wavelength ranges, and the maximum confinement losses of the Y-polarized core modes are up to 79169.3 and 63396.0 dB/m, respectively, while the maximum confinement losses of the X-polarized core modes are only 192.6 and 140.6 dB/m, respectively.

The CLRs of the Si-PCF-1 and the Si-PCF-2 polarization filters are shown in Fig. 10. The wavelength ranges corresponding to the CLR of the Y-polarized and the X-polarized core modes in Fig. 10 are given out in Table 3. From Fig. 10 and the Table 3, when the CLR is larger than 200 times, the wavelength ranges of the Si-PCF-1 and the Si-PCF-2 polarization filters are from 2.66 to 6.80 μm and 3 to 7.80 μm, respectively. When the CLR is larger than 300 times, the wavelength ranges of the Si-PCF-1 and the Si-PCF-2 polarization filters are from 2.73 to 6.77 μm and 3.06 to 7.80 μm, respectively.

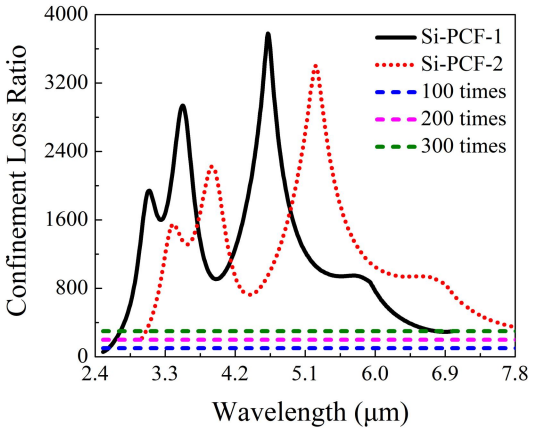

Fig. 11. The CLRs of the Y-polarized and the X-polarized core modes of the Si-PCF-1 and the Si-PCF-2.

Finally, the *ER* and *IL* of the Si-PCF-1 and the Si-PCF-2 polarization filters are shown in Figs. 12(a), 12(b), 12(c), and 12(d), respectively. From Figs. 12(a) and 12(b), the maximum peak value of the *ER* reaches -316 dB when *L* of the Si-PCF-1 is 4 mm. At this time, the wavelength range of the *ER* below -20 dB is from 3.04 to 6.80 μm, and the *IL* is lower than 0.8 dB. From Figs. 12(c) and 12(d), the maximum peak value of the *ER* is -253 dB when *L* of the Si-PCF-2 is 4 mm. At the same time, the wavelength range of the *ER* below -20 dB is from 3.66 to 7.80 μm, where the CLR > 300 times and the *IL* is lower than 0.6 dB.

Table 3. Wavelength Ranges Corresponding to the CLR of the Y-polarized and the X-polarized Core Modes of the Si-PCF-1 and Si-PCF-2.

CLR	Wavelength ranges of the Si-PCF-1 (μm)	Wavelength ranges of the Si-PCF-2 (μm)
CLR > 100 times	2.58~6.80	3.00~7.80
CLR > 200 times	2.66~6.80	3.00~7.80
CLR > 300 times	2.73~6.77	3.06~7.80

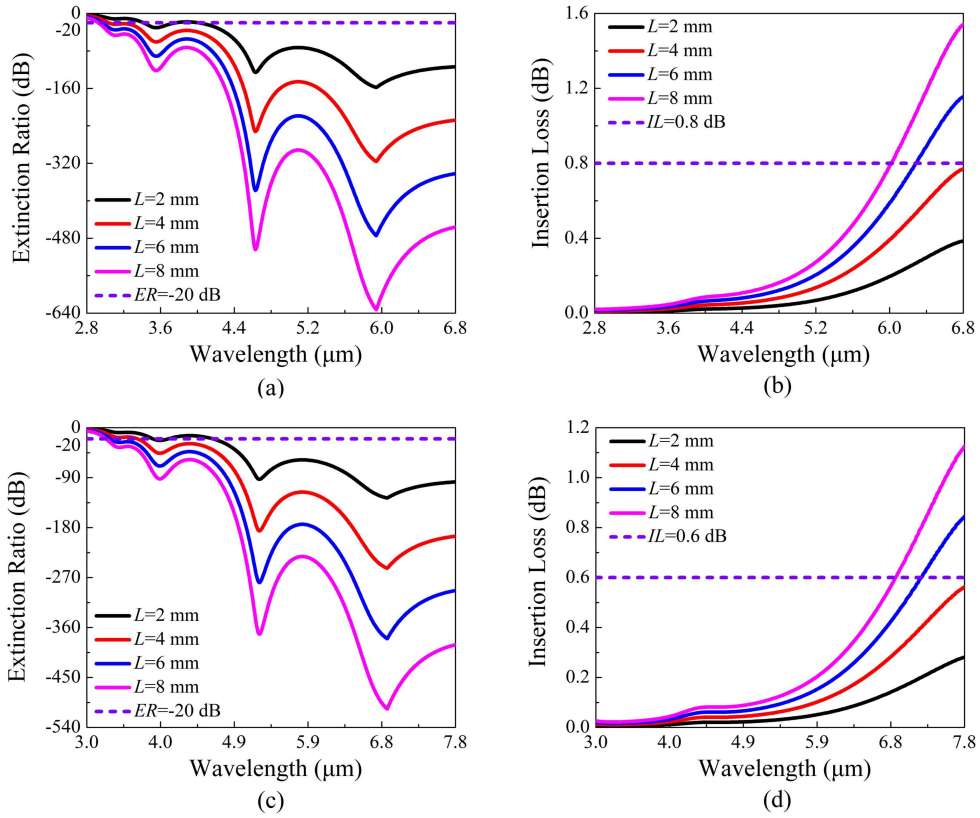

Fig. 12. The relationships between **(a)**, **(c)** *ER* and **(b)**, **(d)** *IL* of the Si-PCF-1 and Si-PCF-2 and wavelength for different *L*.

5. Conclusion

In summary, a mid-infrared Si-PCF polarization filter based on the SPR effect is proposed. The Y-polarized core mode confinement losses at the three resonant wavelengths 2.84, 3.29, and 4.53 μm are 9235.9, 27097.5, and 97818.3 dB/m, respectively. The maximum X-polarized core mode confinement loss is only 234.2 dB/m at wavelength 5.5 μm. The maximum peak value of the extinction ratio reaches -391 dB when *L* of the Si-PCF is 4 mm. Meanwhile, the insertion loss is less than 1 dB and the filter bandwidth is 2.75 μm. By choosing the appropriate fiber structure parameters, the final filtering bandwidth can be obtained within the mid-infrared spectral region of 2.75 to 7.80 μm. The proposed Si-PCF polarization filter has some advantages such as ultra-wide filtering bandwidth, short length, large extinction ratio, and so on and has significant applications in the mid-infrared laser systems.

Acknowledgements

This work was supported in part by the National Key Research and Development Program of China (Granted Nos. 2019YFB2204000) and the National Natural Science Foundation of China (Granted Nos. 61875238 and 61935007).

References

[1] C. Gunasekaran, B. Suneel Kumar, N. Ayyanar, G. Thavasi Raja, R. Mohan, Surface-plasmon-based photonic crystal fibers for high-bandwidth filter realization, J. Opt. Soc. Am. B 36 (2019) 1574-1580.

[2] P. Li, J. L. Zhao, Polarization-dependent coupling in gold-filled dual-core photonic crystal fibers, Opt. Express 21 (2013) 5232-5238 .

[3] X. T. Zhao, L. Hua, Q. Xiong, G. H. Jiang, J. R. Cheng, Ultra-short and broadband polarization splitter based on PCF and metal surface plasmons resonance, Opt. Quant. Electron. 51 (2019) 162.

[4] X. Chen, L. Xia, C. Li, Surface Plasmon Resonance Sensor Based on a Novel D-Shaped Photonic Crystal Fiber for Low Refractive Index Detection, IEEE Photo. J. 10 (2018) 6800709.

[5] C. Liu, L. Yang, X. L. Lu, Q. Liu, F. M. Wang, J. W.i Lv, T. Sun, H. W. Mu, P. K. Chu, Mid-infrared surface plasmon resonance sensor based on photonic crystal fiber, Opt. Express 25 (2017) 14227-14237.

[6] X. Yan,Y. H. L. Gao, T. L. Cheng, S. G. Li, High-loss and broadband photonic crystal fiber polarization filter with two large apertures coated with gold layers, J. Opt. Soc. Am. B 36 (2019) 3085-3089.

[7] B. Y. Li, M. Q. Li, L. Peng, G. Y. Zhou, Z. Y. Hou, C. M. Xia, Research on Dual-Wavelength Single Polarizing Filter Based on Photonic Crystal Fiber, IEEE Photo. J. 9 (2017) 5700209.

[8] J. R. Xue, S. G Li, Y. Z. Xiao, W. Qin, X. J. Xin, X. P. Zhu, Polarization filter characters of the gold-coated and the liquid filled photonic crystal fiber based on surface plasmon resonance, Opt. Express 21 (2013) 13733-13740 .

[9] A. M. Heikal, F. F. K. Hussain, M. F. O. Hameed, S. S. A. Obayya, Efficient Polarization Filter Design Based on Plasmonic Photonic Crystal Fiber, J. Lightw. Technol. 33 (2015) 2868-2875.

[10] Q. Liu, S. G. Li, J. S. Li, C. Dou, X. Y. Wang, G. Y. Wang, M. Shi, Tunable Fiber Polarization Filter by Filling Different Index Liquids and Gold Wire Into Photonic Crystal Fiber, J. Lightw. Technol. 34 (2016) 2484-2490.

[11] M. F. O. Hameed, A. M. Heikal, B. M. Younis, M. Abdelrazzak, S. S. A. Obayya, Ultra-high tunable liquid crystal-plasmonic photonic crystal fiber polarization filter, Opt. Express 23 (2015) 7007-7020.

[12] H. L. Chen, S. G. Li, M. J Ma, Y. C Liu, M. Shi, Q. Liu, T. L. Cheng, Filtering Characteristics and Applications of Photonic Crystal Fibers Being Selectively Infiltrated With One Aluminum Rod, J. Lightw. Technol. 34 (2016) 4972-4980.

[13] C. Liu, L. Y. Wang, F. M. Wang, C. H. Xu, Q. Liu, W. Liu, L.Yang, X. L. Li, T. Sun, P. K. Chu, Tunable single-polarization bimetal-coated and liquid-filled photonic crystal fiber filter based on surface plasmon resonance, Appl. Opt. 58 (2019) 6308-6314.

[14] X. C. Yang, Y. Lu, B. L. Liu, J. Q. Yao, Design of a Tunable Single-Polarization Photonic Crystal Fiber Filter with Silver-Coated and Liquid-Filled Air Holes, IEEE Photo. J. 9 (2017) 7105108.

[15] B. Y. Li, M. Wu, X. Y. Liu, G. Y. Zhou, J. T. Liu, Z. Y. Hou, C. M. Xia, Surface Plasmon Resonance on the V-Type Microstructured Optical Fiber Embedded with Dual Copper Wires, Plasmonics 14 (2019) 383-387.

[16] Y. Guo, J. S. Li, S. G. Li, S. H. Zhang, Y. D. Liu, Broadband single-polarization filter of D-shaped photonic crystal fiber with a micro-opening based on surface plasmon resonance, Appl. Opt. 57 (2018) 8016-8022.

[17] M. Chang, B. X Li, N. Chen, X. L. Lu, X. D. Zhang, J. Xu, A Compact and Broadband Photonic Crystal Fiber Polarization Filter Based on a Plasmonic Resonant Thin Gold Film, IEEE Photo. J. 11(2019) 7202312.

[18] J. Ballato, T. Hawkins, P. Foy, R. Stolen, B. Kokuoz, M. Ellison, C. McMillen, J. Reppert, A. M. Rao, M. Daw, S. Sharma, R. Shori, O. Stafsudd, R. R. Rice, D. R. Powers, Silicon Optical Fiber, Opt. Express 16 (2008) 18675-18683.

[19] C. Hou, X. T. Jia, L. Wei, S. C. Tan, X Zhao, J. D. Joannopoulos, Y. Fink, Crystalline silicon core fibres from aluminium core preforms, Nat. Commun. 6 (2015) 6248.

[20] F. Yaman, H. Pang, X. B. Xie, P. LiKamWa, G. F, Li, Silicon Photonic Crystal Fiber, in Conference on Lasers and Electro-Optics/International Quantum Electronics Conference, OSA Technical Digest (CD) (Optical Society of America, 2009), paper CTuDD7.

[21] Z. H Bao, M. R. Weatherspoon, S. Shian, Y. Cai, P. D. Graham, S. M. Allan, G. Ahmad, M. B. Dickerson, B. C.

Church, Z. T. Kang, H. W. Abernathy III, C. J. Summers, M. L. Liu, K. H. Sandhage, Chemical reduction of three-dimensional silica micro-assemblies into microporous silicon replicas, Nature 446 (2007) 172-175 .

[22] T. Y. Huang, J. F. Liao, S. N. Fu, M. Tang, P. Shum, Slot Spiral Silicon Photonic Crystal Fiber With Property of Both High Birefringence and High Nonlinearity, IEEE Photo. J. 6 (2014), 2200807.

[23] J. F. Liao, Y. M. Xie, X. H. Wang, D. B Li, T. Y. Huang, Ultra-flattened nearly-zero dispersion and ultrahigh nonlinear slot silicon photonic crystal fibers with ultrahigh birefringence, Photo. Nanostruct. 25 (2017) 19-24.

[24] C. Liu, W. Q. Su, Q. Liu, X. L. Lu, F. M. Wang, T. Sun, P. K. Chu, Symmetrical dual D-shape photonic crystal fibers for surface plasmon resonance sensing, Opt. Express 26 (2018), 9039-9049.

[25] R. M. O. Jr, N. C. Panoiu, J. I. Dadap, X. P. Liu, X. G. Chen, I. W. Hsieh, E. Dulkeith, W. M. J. Green, Y. A. Vlasov, Engineering nonlinearities in nanoscale optical systems: physics and applications in dispersion-engineered silicon nanophotonic wires, Adv. Opt. Photo. 1 (2009) 162-235.

[26] Y. W. Qu, J. H. Yuan, X. Zhou, F. Li, C. Mei, B. B. Yan, Q. Wu, K. R. Wang, X. Z. Sang, K. P. Long, C. X. Yu, A V-shape photonic crystal fiber polarization filter based on surface plasmon resonance effect, Opt. Commun. 452 (2019) 1-6.

[27] T. Y. Yang, C. Ding, R. W. Ziolkowski, Y. Jay Guo, A Scalable THz Photonic Crystal Fiber With Partially-Slotted Core That Exhibits Improved Birefringence and Reduced Loss, J. Lightw. Technol. 36 (2017) 3408-3417.

[28] L. H. Jiang, Y. Zheng, J. J. Yang, L. T. Hou, Z. H. Li, X. T. Zhao, An Ultra-broadband Single Polarization Filter Based on Plasmonic Photonic Crystal Fiber with a Liquid Crystal Core, Plasmonics 12 (2017) 411-417.

[29] J. S. Chiang, N. H. Sun, S. C. Lin, W. F. Liu, Analysis of an Ultrashort PCF-Based Polarization Splitter, J. Lightw. Technol. 28 (2010) 707-713.

[30] Q. Liu, S. G. Li, H. L. Chen, Two Kinds of Polarization Filter Based on Photonic Crystal Fiber With Nanoscale Gold Film, IEEE Photo. J. 7 (2015), 2700210.

[31] Z. H. Zhang, Y. F. Shi, B. M. Bian, and J. Lu, Dependence of leaky mode coupling on loss in photonic crystal fiber with hybrid cladding, Opt. Express 16 (2008) 1915-1922.

[32] X. Feng, A. K. Mairaj, D. W. Hewak, T. M. Monro, Nonsilica Glasses for Holey Fibers, J. Lightw. Technol. 23 (2005), 2046-2054.

[33] Y. Li, K. Itoh, W. Watanabe, K. Yamada, D. Kuroda, J. Nishii, Y. Y. Jiang, Three-dimensional hole drilling of silica glass from the rear surface with femtosecond laser pulses, Opt. Lett. 26 (2001) 1912-1914.

[34] C. Hong, H. Kim, S. Park, C. Lee, Optical properties of porous silicon coated with ultrathin gold film by RF-magnetron sputtering, J. Eur. Ceram. Soc. 30 (2010) 459-463.

[35] X. Zhang, R. Wang, F. M. Cox, B.T. Kuhlmey, M. C. J. Large, Selective coating of holes in microstructured optical fiber and its application to in-fiber absorptive polarizers, Opt. Express 15 (2007) 16270-16278.

[36] P. J. A. Sazio, A. A. Correa, C. E. Finlayson, J. R. Hayes, T. J. Scheidemantel, N. F. Baril, B. R. Jackson, D. J. Won, F. Zhang, E. R. Margine, V. Gopalan, V. H. Crespi, J. V. Badding, Microstructured Optical Fibers as High-Pressure Microfluidic Reactors, Science 311 (2006) 1583-1586.

[37] J. Y. Jing, Q. Wang, B. T. Wang, Refractive index sensing characteristics of carbon nanotube-deposited photonic crystal fiber SPR sensor, Opt. Fiber Technol. 43 (2018) 137-144.

[38] T. S. Wu, Y. Shao, Y. Wang, S. Q. Cao, W. P. Cao, F. Zhang, C. R. Liao, J. He, Y. J. Huang, M. X. Hou, Y. P. Wang, Surface plasmon resonance biosensor based on gold-coated side-polished hexagonal structure photonic crystal fibe, Opt. Express 25 (2017) 20313-20322.

[39] Y. Wang, Q. Huang, W. J. Zhu, M. H. Yang, E. Lewis, Novel optical fiber SPR temperature sensor based on MMF-PCF-MMF structure and gold-PDMS film, Opt. Express 26 (2018) 1910-1917.